



HAL
open science

Comparison of results on N_{eff} from various Planck likelihoods

Sophie Henrot-Versillé, Francois Couchot, Xavier Garrido, Hiroaki Imada,
Thibaut Louis, Matthieu Tristram, Sylvain Vanneste

► **To cite this version:**

Sophie Henrot-Versillé, Francois Couchot, Xavier Garrido, Hiroaki Imada, Thibaut Louis, et al.. Comparison of results on N_{eff} from various Planck likelihoods. *Astronomy and Astrophysics - A&A*, 2019, 623, pp.A9. 10.1051/0004-6361/201834060 . hal-01851160

HAL Id: hal-01851160

<https://hal.science/hal-01851160>

Submitted on 18 Nov 2020

HAL is a multi-disciplinary open access archive for the deposit and dissemination of scientific research documents, whether they are published or not. The documents may come from teaching and research institutions in France or abroad, or from public or private research centers.

L'archive ouverte pluridisciplinaire **HAL**, est destinée au dépôt et à la diffusion de documents scientifiques de niveau recherche, publiés ou non, émanant des établissements d'enseignement et de recherche français ou étrangers, des laboratoires publics ou privés.

Comparison of results on N_{eff} from various *Planck* likelihoods

S. Henrot-Versillé, F. Couchot, X. Garrido, H. Imada, T. Louis, M. Tristram, and S. Vanneste

LAL, Univ. Paris-Sud, CNRS/IN2P3, Université Paris-Saclay, Orsay, France
e-mail: versille@lal.in2p3.fr

Received 9 August 2018 / Accepted 29 November 2018

ABSTRACT

In this paper, we study the estimation of the effective number of relativistic species from a combination of cosmic microwave background (CMB) and baryon acoustic oscillations (BAO) data. We vary different ingredients of the analysis: the *Planck* high- ℓ likelihoods, the Boltzmann solvers, and the statistical approaches. The variation of the inferred values gives an indication of an additional systematic uncertainty, which is of the same order of magnitude as the error derived from each individual likelihood. We show that this systematic uncertainty is essentially associated to the assumptions made in the high- ℓ likelihood implementations, in particular for the foreground residuals modellings. We also compare a subset of likelihoods using only the TE power spectra, expected to be less sensitive to foreground residuals.

Key words. cosmological parameters

1. Introduction

The expansion rate in the early universe depends on the energy density of relativistic particles, which is parameterised by N_{eff} , the effective number of relativistic species or degrees of freedom. According to the standard model (SM) of particle physics, N_{eff} should only receive contributions from the three neutrino species. Due to residual interactions, as the neutrinos were not completely decoupled during the electron-positron annihilation, N_{eff} is expected to be equal to 3.045 (de Salas & Pastor 2016).

Any deviation from the SM value can be attributed to extra relativistic radiation in the early universe. This can be, for example, massless sterile neutrino species (Hamann et al. 2010), axions (Melchiorri et al. 2007; Hannestad et al. 2010), decay of non-relativistic matter (Fischler & Meyers 2011), gravitational waves (Smith et al. 2006; Henrot-Versillé et al. 2015), extra dimensions (Binetruy et al. 2000; Shiromizu et al. 2000; Flambaum & Shuryak 2006), early dark energy (Calabrese et al. 2011), asymmetric dark matter (Blennow et al. 2012), or leptonic asymmetry (Caramete & Popa 2014). Accurately measuring N_{eff} is therefore of particular interest not only to constrain neutrino physics but also any other process that changes the expansion history.

Any variation of the expansion rate of the universe affects the cosmic microwave background (CMB) power spectra by changing the relative scales of the Silk damping relative to the sound horizon (see e.g. Abazajian et al. 2015). Therefore, the current best constraint on N_{eff} comes from the accurate measurements of the temperature and polarisation anisotropies performed by *Planck*.

In this paper we discuss in detail the estimation of N_{eff} from CMB data and quantify the dependence of the results on the choices made in the analysis. We investigate different possible sources of systematic errors. We first compare the results obtained using two Boltzmann codes: CAMB (Lewis et al. 2000) and CLASS (Blas et al. 2011). We then use three different *Planck* high- ℓ likelihoods. We also discuss the statistical analysis, comparing the frequentist and Bayesian approaches, to pinpoint any

remaining volume effects. We show that varying the above-listed ingredients leads to a non-negligible spread of the mean N_{eff} values.

The paper is organised as follows. In Sect. 2, we introduce the datasets, the *Planck* likelihoods, the Boltzmann codes, and the statistical analysis. In Sect. 3, we quantify the effect of possible sources of systematic error on N_{eff} using the combination of temperature and polarization CMB data (TT + TE + EE) together with baryon acoustic oscillation (BAO) data. In Sect. 4, we compare the results obtained with the CMB TT and TE power spectra. The conclusions are given in Sect. 5.

2. Phenomenology and methodology

2.1. Introduction

N_{eff} relates the radiation (Ω_{rad}) and the photon (Ω_{γ}) energy densities relative to the critical density through:

$$\Omega_{\text{rad}} = \left(1 + \frac{7}{8} N_{\text{eff}} \left(\frac{4}{11} \right)^{4/3} \right) \Omega_{\gamma}. \quad (1)$$

Under the assumption that only photons and standard light neutrinos contribute to the radiation energy density, N_{eff} is equal to the effective number of neutrinos: $N_{\text{eff}} \simeq 3.045$. This value has been derived from the number of neutrinos constrained by the measurement of the decay width of the Z boson (Beringer 2012), and takes into account residual interactions during the electron-positron annihilation.

2.2. Data sets and likelihoods

The datasets and likelihoods used in this paper are summarized together with their corresponding acronyms in Table 1. Several high- ℓ (respectively low- ℓ) likelihoods have been derived from the *Planck* 2015 data (Planck Collaboration XI 2016; Couchot et al. 2017a; Planck Collaboration Int. XLVII 2016) and are further described in Sect. 2.2.2 (respectively Sect. 2.2.1). The BAO data are also discussed in Sect. 2.2.3.

Table 1. Summary of keywords, data, and likelihoods together with their corresponding acronyms used in this paper.

Acronym	Description
hlpXXps	High- ℓ HiLLiPOPps <i>Planck</i> likelihood
CamSpec	Cambridge high- ℓ <i>Planck</i> likelihood
Plik	Public high- ℓ <i>Planck</i> likelihood
hlpXX	High- ℓ HiLLiPOPps <i>Planck</i> likelihood (one point source amplitude per cross-spectrum)
hlpXXps(Plik-like)	High- ℓ HiLLiPOPps <i>Planck</i> likelihood (see Sect. 3.2.1)
TT	Refers to the temperature power spectra
TE	Refers to the temperature and E modes cross-spectra
EE	Refers to the E modes power spectra
ALL	Refers to the combination of temperature and polarisation CMB data (incl. TT, TE, and EE)
Comm	Commander low- ℓ temperature <i>Planck</i> public likelihood
lowTEB	Pixel-based temperature and polarisation low- ℓ <i>Planck</i> public likelihood
BAO	Baryon Acoustic Oscillation data (cf. Sect. 2.2.3)
PLA	Planck Legacy Archive

Notes. Plik, Commander, lowTEB are the public likelihoods delivered by the *Planck* consortium. See text for detail and references.

2.2.1. Low- ℓ likelihoods

At low multipoles ($\ell < 50$), the *Planck* public likelihood is lowTEB, based on *Planck* Low Frequency Instrument (LFI) maps at 70 GHz for polarization and a component-separated map using all *Planck* frequencies for temperature (Commander [Planck Collaboration XI 2016](#)).

In the following, we also test a combination of the Lollipop likelihood (Mangilli et al. 2015) with Commander in place of lowTEB, following what has been done for the latest *Planck* results on the reionisation optical depth ([Planck Collaboration Int. XLVII 2016](#)).

2.2.2. High- ℓ likelihoods

At high multipoles ($\ell > 50$), different likelihoods were developed within the *Planck* collaboration: Plik ([Planck Collaboration XI 2016](#)) being the one delivered to the community. Their implementations are further detailed in this section. Since there is no valuable reason to favour one implementation over another, we use them in the following to assess the impact of the various ingredients entering their derivation on the N_{eff} inferred value. We consider Plik, CamSpec ([Planck Collaboration XI 2016](#)), and HiLLiPOPps.

All these likelihoods are based on pseudo- C_ℓ cross-spectra between *Planck* High Frequency Instrument (HFI) half-mission maps at 100, 143, and 217 GHz (for more details, see [Planck Collaboration XI 2016](#)). The main differences are listed below:

Data. HiLLiPOPps makes use of all 15 cross-spectra from the six half-mission maps whereas Plik and CamSpec remove the 100×143 and 100×217 correlations together with two of the four 143×217 cross-spectra (for temperature data only). To avoid residual contamination from dust emission, HiLLiPOPps and CamSpec do not use the multipoles below 500 for the 143×217 and 217×217 cross-spectra.

Masks. The Galactic masks used in temperature are very similar. Still, HiLLiPOPps relies on a more refined procedure for the point-source masks that preserves Galactic compact structures and ensures the completeness level at each frequency, but with a higher detection threshold (thus leaving more extra-Galactic diffuse sources as residuals). In polarization, CamSpec uses a cut in polarization amplitude ($P = \sqrt{Q^2 + U^2}$) to define

diffuse Galactic polarization masks whereas HiLLiPOPps and Plik use the same masks as in temperature.

Covariance matrix. The approximations used to calculate the covariance matrix which encompasses the ℓ -by- ℓ correlations between all the cross-power spectra are slightly different. Plik and CamSpec assume a model for signal (from cosmological and astrophysical origin) and noise (with slight differences in the methods used to estimate noise). In HiLLiPOPps, it is estimated semi-analytically with Xpol (a polarized version of the power spectrum estimator described in [Tristram et al. 2005](#)) using a smoothed version of the estimated spectra ([Couchot et al. 2017a](#)).

Galactic dust template. HiLLiPOPps uses templates for the Galactic dust emission derived from *Planck* measurements both for the shape of the power spectra ([Planck Collaboration Int. XXX 2016](#)) and for the spectral energy distribution (SED; [Planck Collaboration Int. XXII 2015](#)), rescaled by one amplitude for each polarisation mode (TT, EE and TE). In contrast, due to Galactic cirrus residuals that are included in their point-source masks, Plik and CamSpec have to rely on an empirical fit of the spectrum mask difference at 545 GHz and fit one amplitude for each of the cross-frequency spectra with priors on the amplitude based on a power-law (with slightly different spectral index: -2.63 for Plik and -2.7 for CamSpec). In polarization, CamSpec compresses all the frequency combinations of TE and EE spectra into single TE and EE spectra (weighted by the inverse of the diagonals of the appropriate covariance matrices), after foreground cleaning using the 353 GHz maps. As a consequence, CamSpec has no nuisance parameters describing polarized Galactic foregrounds.

SZ template. The template spectra for thermal Sunyaev-Zeldovich (SZ) effect residuals is based on a model for Plik and CamSpec; whereas it comes directly from *Planck* measurements in the case of HiLLiPOPps.

Point-source template. HiLLiPOPps includes a two-component point-source model (including infrared dusty galaxies and extragalactic radio sources) with one amplitude for each component and a fixed SED whereas all the other likelihoods fit one point-source amplitude for each cross-frequency. We also consider a version which fits one point-source amplitude per cross-spectrum (as what is done in Plik), labelled HiLLiPOP.

The results obtained with those high- ℓ likelihoods have been compared in [Planck Collaboration XI \(2016\)](#) when combined with a prior on the optical depth to reionization (τ_{reio}). It was shown that the Λ CDM parameters derived from temperature data were very compatible. Still, as described in [Couchot et al. \(2017b\)](#), when combining them with lowTEB, a disagreement was observed, especially on τ_{reio} and A_s (the initial super-horizon amplitude of curvature perturbations at $k = 0.05 \text{ Mpc}^{-1}$). This was shown to be related to a discrepancy on the A_L fitted value: A_L is a phenomenological parameter that was first introduced in [Calabrese et al. \(2008\)](#) to cross-check the consistency of the data with the Λ CDM model. Further studies on the impact of those differences on the measurement of the sum of the neutrino mass were also performed in [Couchot et al. \(2017c\)](#).

In the following we investigate the systematic effects hidden in the assumptions made for the derivation of those likelihoods. As the use of a single likelihood does not ensure the full propagation of errors, we base our analysis on a comparison of the results inferred from each of them and estimate the order of magnitude of the related errors.

2.2.3. Baryon acoustic oscillation (BAO) data

Information on the late-time evolution of the universe geometry is also included. In this work, we use the acoustic-scale distance ratio $D_V(z)/r_{\text{drag}}$ measurements from the 6dF Galaxy Survey at $z = 0.1$ ([Beutler et al. 2014](#)).

$D_V(z)$ is a combination of the comoving angular diameter distance $D_M(z)$ and Hubble parameter $H(z)$ according to:

$$D_V(z) = \left[D_M^2(z) \frac{cz}{H(z)} \right]^{1/3}, \quad (2)$$

and r_{drag} is the comoving sound horizon at the end of the baryonic-drag epoch. At higher redshift, we have also included the BOSS DR12 BAO measurements ([Alam et al. 2017](#)). They consist in constraints on $(D_M(z), H(z), f(z)\sigma_8(z))$ in three redshift bins, which encompass both BOSS-LowZ and BOSS-CMASS DR11 results. The factor $\sigma_8(z)$ gives the normalization of the linear theory matter power spectrum at redshift z on $8 h^{-1} \text{ Mpc}$ scales and $f(z)$ is the derivative of the logarithmic growth rate of the linear fluctuation amplitude with respect to the logarithm of the expansion factor. The combination of those measurements is labelled BAO in the following. We note that this is an update of the BAO data with respect to those used in [Planck Collaboration XIII \(2016\)](#).

2.3. Statistics and Boltzmann codes

We use the CAMEL software¹ ([Henrot-Versillé et al. 2016](#)) tuned to a high precision setting to perform the statistical analysis. It allows us to compare both the frequentist (profile likelihoods) and the Bayesian approaches. CAMEL includes a MCMC algorithm based on the Adaptive Metropolis method ([Haario et al. 2001](#)). It also encapsulates the CLASS Boltzmann solver ([Blas et al. 2011](#)). The CLASS and CAMB softwares have been extensively compared ([Lesgourgues 2011](#)), and lead to very close predictions in terms of CMB spectra. Still, the public *Planck* results are derived using CAMB: their comparison with the ones derived with CAMEL allows us to cross-check the compatibility of the theoretical predictions while fitting for N_{eff} .

For both setups, we are using the model of [Takahashi et al. \(2012\)](#) extended to massive neutrinos as described in [Bird](#)

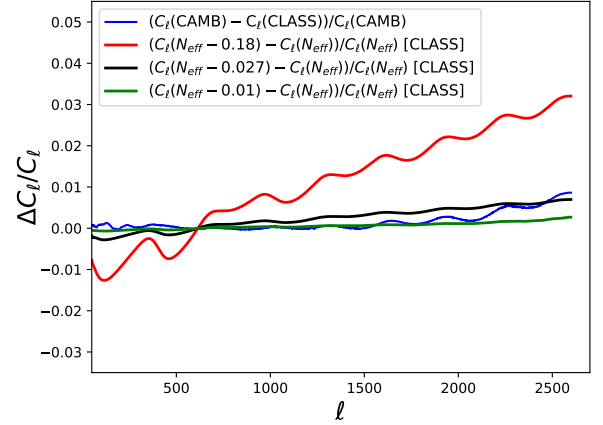


Fig. 1. Relative variations of the predicted temperature spectra between CLASS and CAMB (blue). We also compare the spectra when we shift N_{eff} toward negative values for $\Delta N_{\text{eff}} = -0.18$ (red), $\Delta N_{\text{eff}} = -0.027$ (black), and $\Delta N_{\text{eff}} = -0.01$ (green) with CLASS (θ is fixed, H_0 is therefore recalculated).

[et al. \(2012\)](#) to include non-linear effects on the matter power spectrum evolution. We have used the big-bang nucleosynthesis (BBN) predictions calculated with the PArthENoPE code ([Consiglio et al. 2018](#)) updated to the latest observational data on nuclear rates and assuming a neutron lifetime of 880.2 s, identical to the standard assumptions made in [Planck Collaboration XIII \(2016\)](#).

For Λ CDM, we assume that all the neutrino mass ($\Sigma m_\nu = 0.06 \text{ eV}$) is carried out by only one heavy neutrino. Considering current knowledge of the neutrino sector ([Tanabashi et al. 2018](#)), we do not yet have access to a measurement of the individual masses. Two mass hierarchy scenarios are therefore considered in the literature: the normal hierarchy with $m_1 < m_2 \ll m_3$ and the inverted hierarchy with $m_3 \ll m_1 < m_2$, where m_i ($i = 1; 2; 3$) denotes the neutrino mass eigenstates. In this paper, we have also performed fits with three neutrinos with a mass splitting scheme derived from the normal hierarchy (keeping $\Sigma m_\nu = 0.06 \text{ eV}$) and obtain identical results.

We illustrate in [Fig. 1](#) the relative variations of the temperature spectra ($\Delta C_\ell/C_\ell$) between CAMB and CLASS. We show the impact of a negative shift of the N_{eff} value in three cases: $\Delta N_{\text{eff}} = -0.18$ corresponding to the 1σ error reported by *Planck*, $\Delta N_{\text{eff}} = -0.027$ which is the forecasted uncertainty for the next generation ‘‘Stage-4’’ ground-based CMB experiment, CMB-S4 ([Abazajian et al. 2016](#)), and $\Delta N_{\text{eff}} = -0.01$ which is close to the CAMB/CLASS difference. The non-linear effects have been deliberately neglected to produce this figure.

3. TT+TE+EE+BAO results

In this section, we discuss the results obtained with the combination of *Planck* TT+TE+EE (so-called ALL) likelihoods together with BAO data. They are given in [Table 2](#), and are classified according to various kinds of systematic errors. Each of them is further discussed in a dedicated subsection below: we first assess the impact of the choice of the Boltzmann solver, then we discuss the impact of the choice of the high- ℓ likelihood. Finally we compare the results using different statistical analysis.

All the values which are tagged with a ‡ are extracted from the PLA.

¹ camel.in2p3.fr

Table 2. Results on N_{eff} obtained when combining PlikALL, hlpALL and hlpALLps with BAO.

	<i>Planck</i> \mathcal{L} +lowTEB+BAO	Config	N_{eff}
1	PlikALL [#]	MCMC/CAMB	3.04 ± 0.18
<i>Boltzmann code and sampler systematics</i>			
2	PlikALL	MCMC/CLASS	$3.03_{-0.17}^{+0.17}$
<i>Likelihood systematics</i>			
3	CamSpecALL [#]	MCMC/CAMB	2.89 ± 0.19
4	hlpALL	MCMC/CLASS	$2.92_{-0.15}^{+0.15}$
5	hlpALLps	MCMC/CLASS	$2.86_{-0.15}^{+0.14}$
<i>Statistical analysis systematics</i>			
6	PlikALL	Profile/CLASS	$3.00_{-0.20}^{+0.19}$
7	hlpALL	Profile/CLASS	$2.87_{-0.14}^{+0.15}$
8	hlpALLps	Profile/CLASS	2.85 ± 0.14
9	hlpALLps (Plik-like)	Profile/CLASS	$2.90_{-0.16}^{+0.17}$

Notes. Errors are given at 68% CL. lowTEB has been used at low- ℓ .

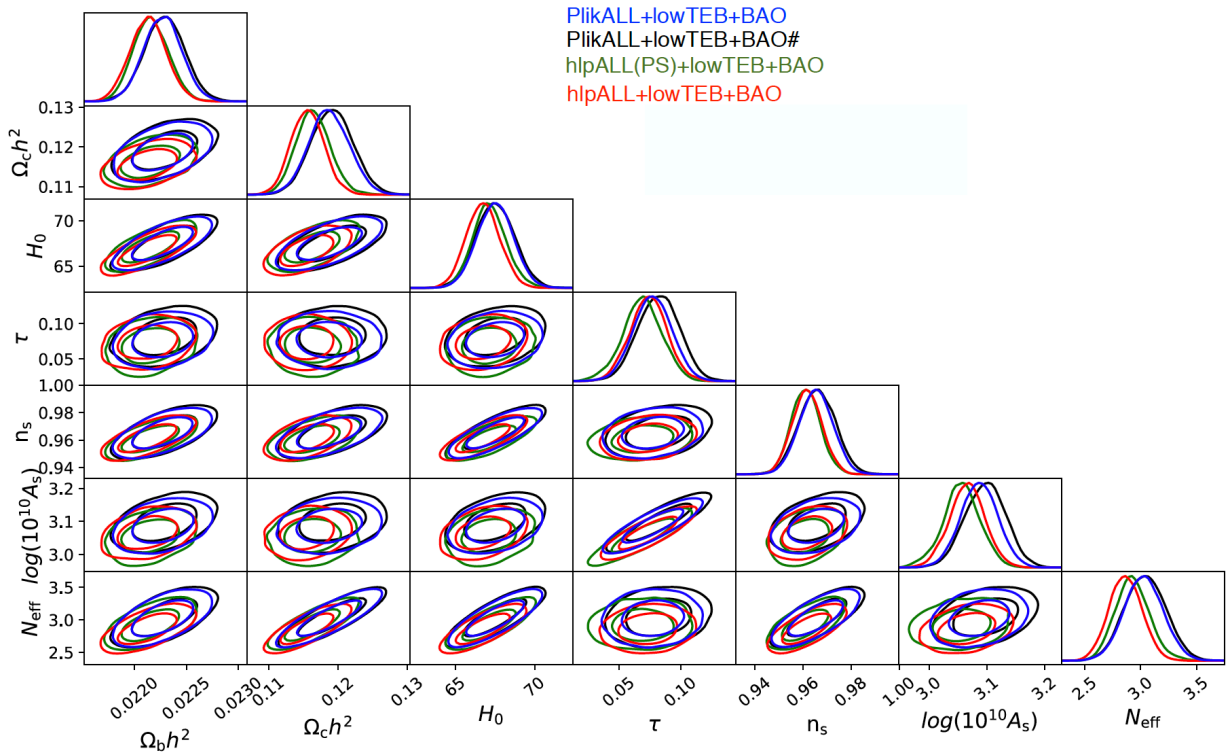


Fig. 2. Cosmological parameters obtained with a combination of lowTEB, BAO, and high- ℓ likelihoods: HiLLiPOP, HiLLiPOPps, Plik/CLASS, and Plik/CAMB (the chains are the ones of the PLA using CAMB).

3.1. Boltzmann code and sampler effects

In this subsection, we study the impact of the choice of the Boltzmann solver that is used to infer cosmological parameters. Within our setup we cannot disentangle the impact of the Boltzmann code from the one of the sampler used for the MCMC mutiparameter space exploration, as a consequence the estimation given in this section combines both effects.

The comparison of the results using Plik are given in Table 2 (line 1 and 2): the use of CLASS combined with the CAMEL MCMC sampler tends to induce slightly smaller error bars on N_{eff} as well as a very small shift of 0.01 toward lower values when results are compared with the public *Planck* results; this effect is further illustrated by the difference between the

black (for the public/CAMB) and the blue (for this work/CLASS) marginalized distributions on cosmological parameters shown on Fig. 2 (see following section for a full description of the figure). This shift is consistent with the difference shown on Fig. 1 between spectra predicted by both Boltzmann solvers, and is largely subdominant compared to the statistical uncertainty.

We also tested the effect of changing the neutrino model. We have compared the results when attributing to each of the three neutrinos a mass derived from the Normal Hierarchy scenario expectation and found a 0.01 shift of the N_{eff} results. Given the actual precisions on the CMB spectra, we can therefore safely assume a Λ CDM model with only one massive neutrino carrying all the mass.

Table 3. Results on MCMC chains for all cosmological parameters obtained when combining the PlikALL, hlpALL, and hlpALLps *Planck* likelihoods with lowTEB and BAO.

Param	hlpALL(CLASS)	hlpALLps(CLASS)	PlikALL(CLASS)	PlikALL(CAMB) [#]
$\Omega_b h^2$	0.02215 ^{-0.00017} _{+0.00018}	0.02213 ^{-0.00018} _{+0.00017}	0.02227 ^{-0.00018} _{+0.00018}	0.02229 ^{-0.00019} _{+0.00019}
$\Omega_c h^2$	0.1163 ^{-0.0023} _{+0.0025}	0.1155 ^{-0.0023} _{+0.0023}	0.1187 ^{-0.0029} _{+0.0030}	0.1191 ^{-0.0031} _{+0.0030}
H_0	67.14 ^{-1.01} _{+1.074}	66.71 ^{-1.02} _{+1.058}	67.51 ^{-1.13} _{+1.125}	67.49 ^{-1.21} _{+1.235}
τ_{reio}	0.069 ^{-0.016} _{+0.016}	0.074 ^{-0.015} _{+0.014}	0.077 ^{-0.016} _{+0.016}	0.082 ^{-0.017} _{+0.017}
n_s	0.961 ^{-0.006} _{+0.006}	0.962 ^{-0.006} _{+0.006}	0.965 ^{-0.007} _{+0.007}	0.966 ^{-0.008} _{+0.008}
$\ln(10^{10} A_s)$	3.06 ^{-0.03} _{+0.03}	3.07 ^{-0.03} _{+0.03}	3.09 ^{-0.03} _{+0.03}	3.10 ^{-0.04} _{+0.03}
N_{eff}	2.92 ^{-0.15} _{+0.15}	2.86 ^{-0.14} _{+0.15}	3.03 ^{-0.17} _{+0.17}	3.04 ^{-0.18} _{+0.18}

Notes. Errors are given at 68% CL.

3.2. Likelihood comparisons

3.2.1. Results

A possible source of systematic error to be estimated is related to the choice of the *Planck* high- ℓ likelihood. As discussed in Sect. 2.2, various assumptions have been made to build the likelihood. The comparison of the results from each likelihood allows for the impact of the underlying assumptions to be quantified.

A discrepancy between PlikALL and CamSpecALL is already mentioned in *Planck Collaboration XIII* (2016), which quotes $\Delta N_{\text{eff}} \simeq 0.15$. Using the HiLLiPOP likelihoods, we find differences of the same order of magnitude as quoted in Table 2 (line 1 vs. lines 3, 4, 5). This variation can reach a maximum of $\Delta N_{\text{eff}} \simeq 0.17$.

However, as stated in Sect. 2.2, there are more data in the HiLLiPOPps likelihoods than in Plik and CamSpec. This can affect the interpretation of the shift, as part of it might be due to statistical fluctuations. To test this effect, we have derived the results using HiLLiPOP while removing the 100×143 , 100×217 , and two of the four 143×217 cross-spectra, and reducing the ℓ range (see Sect. 2.2.2): the result is quoted on line 9 and labelled HiLLiPOPps(Plik-like). We see that a small part (up to 0.03) of the value of 0.17 may be attributed to a statistical effect (including the covariance matrix determination).

3.2.2. Correlations with other parameters

In this section we investigate the correlation between N_{eff} and the cosmological and nuisance parameters, the definition of the latter being given in Table A.1. For hlpTTps, the model for the point-source residuals is slightly different (see Sect. 2.2.2): A_{radio} and A_{dusty} are respectively the amplitudes of the radio sources and the dusty galaxies (Couchot et al. 2017a). The nuisance parameters for Plik are further defined in *Planck Collaboration XV* (2014) and *Planck Collaboration XI* (2016). The cosmological parameters we infer together with N_{eff} are the sixth parameters of the base Λ CDM model, as defined in *Planck Collaboration XVI* (2014), namely:

- $\Omega_b h^2$: Today’s baryon density,
- $\Omega_c h^2$: Today’s cold dark matter density,
- H_0 : Current expansion rate in $\text{km s}^{-1} \text{Mpc}^{-1}$,
- τ_{reio} : Optical depth to reionization,
- n_s : Scalar spectrum power-law index,
- $\ln(10^{10} A_s)$: Log power of the primordial curvature perturbations.

We give on Table 3 and Fig. 2 the results of the CAMEL MCMC sampler using the CLASS Boltzmann solver with PlikALL, hlpALL, and hlpALLps (combined with lowTEB and BAO)

compared to the *Planck* public chains for N_{eff} , plus the six Λ CDM parameters. Similarly to what is observed on N_{eff} , we find variations of the parameters between likelihoods of the order of one sigma or less. The error bars of the HiLLiPOPps likelihoods are slightly smaller due to the additional data that are used (see Sect. 2.2.2).

The correlations between N_{eff} and the nuisance parameters are illustrated on Fig. 3 for the three likelihoods (from top to bottom: hlpALL, hlpALLps, PlikALL). For HiLLiPOP, the highest values of the coefficients are obtained for the nuisance parameters related to foregrounds which play a role at small scales: namely the point sources (with a “PS” label in the name of the parameter) and/or the SZ sector. N_{eff} is anti-correlated to the point source parameters when the related nuisance parameters are left free to vary (as this is the case of HiLLiPOPps). Conversely, adding information in the point source model (as done in HiLLiPOPps), this relation is broken. We also observe a correlation between N_{eff} , A_{KSZ} (the amplitude of the kinetic SZ effect), and A_{SZxCIB} (the amplitude of the correlation between SZ and the cosmic infrared background - CIB) but those parameters are only very slightly constrained with *Planck* data. For Plik, the correlation level is lower for all nuisance parameters, but the number of parameters is higher.

3.3. Statistical analysis systematics

3.3.1. Results

In this section, we study the impact of the choice of the statistical analysis (Bayesian vs. frequentist). The main purpose of such a comparison is to check for any volume effect that may significantly impact the results (see e.g. Hamann 2012). The N_{eff} estimates for various *Planck* likelihoods using profile likelihoods are given on lines 6 to 8 of Table 2. A visual comparison of the results is shown on Fig. 4, where the profile analysis results are transformed in terms of $\mathcal{L}/\mathcal{L}_{\text{max}}$ and are superimposed on the MCMC posterior distributions.

The profile analysis results systematically lead to smaller mean values, keeping the error bars almost similar. This effect is also present in the PLA: for example, the N_{eff} values extracted from the best-fit procedure (which is exactly what is done in a profile analysis) quoted for the PlikALL+lowTEB+BAO combination is equal to 2.996, a value which is $\simeq 0.04$ smaller than the maximum of the MCMC posterior distributions. The variation is specific to each likelihood and not expected to be constant as it reflects its very shape in the multidimensional parameter space. The higher volume effect is observed for HiLLiPOP and does not exceed $\Delta N_{\text{eff}} = 0.05$.

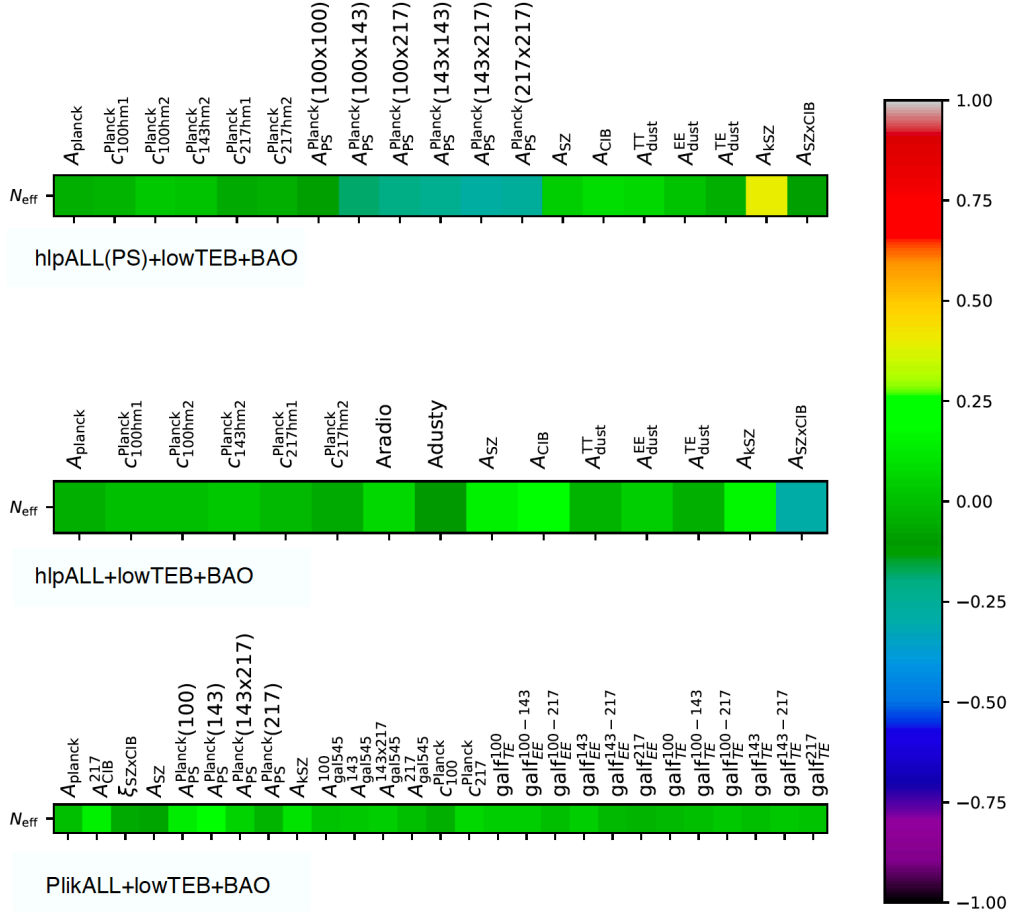


Fig. 3. Correlation coefficients between N_{eff} and the nuisance parameters from *top to bottom* for hlpALL, hlpALLps, and PlikALL when combined with BAO and lowTEB.

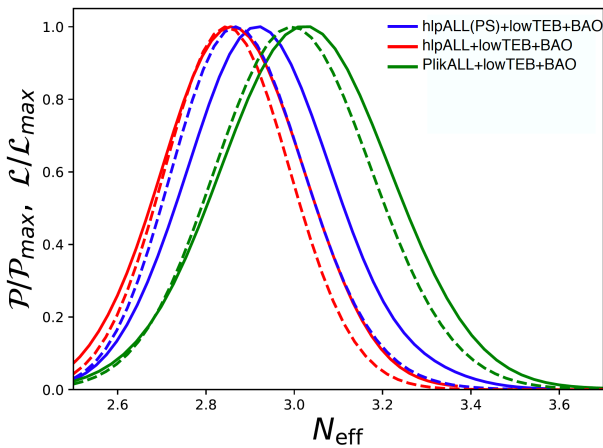


Fig. 4. Posterior distributions of the MCMC analysis (plain lines) and Profile likelihood ratio $\mathcal{L}/\mathcal{L}_{\text{max}}$ (dashed lines) for hlpALL (blue), hlpALLps (red), and PlikALL (green) combined with lowTEB+BAO.

3.3.2. Statistical and nuisance error contribution

Following the procedure described in Aad (2014), we have separately estimated the two contributions to the total error: the one coming from statistics and the one linked to the foreground and instrumental modelling (so-called nuisance error). We first built the usual profiles for each likelihood: they are shown in solid lines on Fig. 5 and the corresponding results are given in lines 6 to 8 of Table 2. In a second step, we built another set of pro-

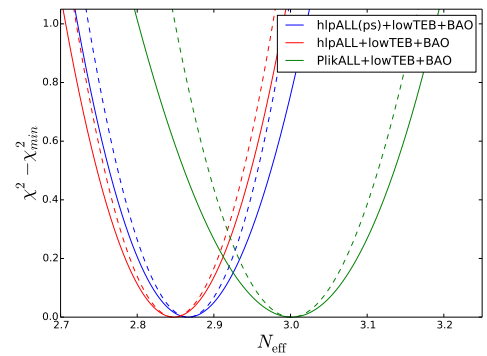


Fig. 5. Comparison of profile likelihoods obtained for the combination of hlpALL (blue), hlpALLps (red), and PlikALL (green) together with BAO and lowTEB. The superimposed dashed profiles were obtained when fixing the nuisance parameter values to the ones obtained for the best fit of each likelihood combination.

files, fixing the nuisance parameters to the values of the previously obtained best-fit. The errors derived from this second fit (shown by a dashed line in Fig. 5) correspond to the ultimate error one would obtain if the precise nuisance parameters were known (and they had the values given by the best-fit). Finally the nuisance error of each individual likelihood is deduced by quadratically subtracting the statistical uncertainty from the total error. The results are given in Table 4.

From the comparison of the results of hlpALLps (Plik-like) and hlpALL, we can deduce that the additional data induce a

Table 4. Full error on N_{eff} and contributions from statistics and nuisance, derived using profile likelihoods and CLASS (see a description of the procedure in Sect. 3.3.2) obtained when combining PlikALL, hlpALL, and hlpALLps with lowTEB and BAO.

<i>Planck</i> \mathcal{L} lowTEB+BAO	Mean value	Full error	Stat error	Nuisance error
PlikALL	3.00	+0.19 -0.20	+0.16 -0.15	+0.12 -0.13
hlpALL	2.87	+0.15 -0.14	± 0.13	+0.06 -0.05
hlpALLps	2.85	± 0.14	± 0.13	+0.05 -0.05
hlpALLps(Plik-like)	2.90	+0.17 -0.16	+0.16 -0.15	+0.05 -0.05

slight shift ($\Delta N_{\text{eff}} = 0.03$), apart from the expected reduction of the statistical error.

From the comparison of the results of hlpALLps(Plik-like) and PlikALL, we observe that the statistical error is exactly the same: giving high confidence to the fact that the impact of the different choices made in the likelihood implementation for the covariance matrix is negligible. The remaining difference, which happens to be the bigger one, comes from the effect of the foreground modelling, which impacts both the mean value and the nuisance error. The foreground modelling (but a different one) is also tested through the comparison of the results of hlpALL and hlpALLps.

3.4. Other cosmological data

We have further tested the impact of CMB Lensing on the N_{eff} measurement and found it to be very small, as expected (cf. [Planck Collaboration XIII 2016](#)), slightly lowering the overall results by 0.01.

We have also checked that the choice of the low- ℓ likelihood had no impact on the final results (replacing lowTEB with Lollipop+Commander as stated in Sect. 2.2.1).

It must be noted that the supernova data do not help to further constrain N_{eff} once the BAO data are used. We therefore chose not to use them in this analysis. For completeness we note that the update of the BAO data from DR11 to DR12 does not impact the constraint on N_{eff} ([Alam et al. 2017](#)).

3.5. Summary

The results on N_{eff} are summarized in Fig. 6. The shift of the mean values observed when using one likelihood or another is of the same order of magnitude as the error derived from each individual likelihood ($\Delta N_{\text{eff}} \simeq 0.17$ vs. $\sigma(N_{\text{eff}}) = 0.18$). This shift has been shown to be mainly driven by the assumptions made for the foreground modelling. A small part of this variation (up to 0.03) has been identified as being linked to the data considered in HiLLiPOP and not in Plik. Still, it is high enough not to be neglected when constraining theoretical models from the N_{eff} measurement only.

4. Fitting TT and TE separately

In the previous sections we have shown the results of the combination of temperature and polarisation CMB data. In the following, we estimate N_{eff} for TT and TE separately to further compare the outcome of each likelihood.

4.1. TT+lowTEB+BAO results

In this section, we consider the combination of temperature-only CMB likelihoods, together with BAO data. The results are sum-

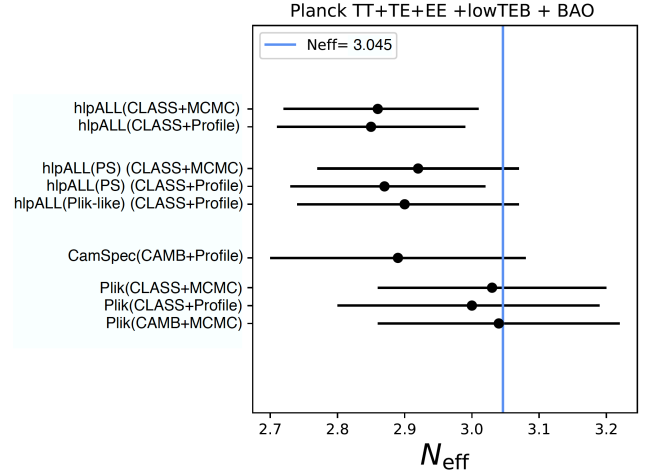


Fig. 6. Comparison results for the combination of *Planck* TT+TE+EE likelihoods, with lowTEB and BAO.

Table 5. Results on N_{eff} obtained when combining PlikTT, hlpTT, and hlpTTps with BAO.

<i>Planck</i> \mathcal{L} +lowTEB+BAO	Config	N_{eff}
PlikTT [#]	MCMC/CAMB	3.15 ± 0.23
PlikTT	Profile/CLASS	$3.09^{+0.21}_{-0.22}$
hlpTT	Profile/CLASS	$3.27^{+0.28}_{-0.26}$
hlpTTps	Profile/CLASS	$3.20^{+0.21}_{-0.20}$

Notes. Errors are given at 68% CL. lowTEB has been used at low- ℓ .

marized in Table 5 for various configurations. For this specific combination the CamSpec results are not public, and therefore we cannot use them in the comparison.

From Table 5, we obtain $\Delta N_{\text{eff}} \simeq 0.18$ from the largest difference observed between hlpTT-Profile/CLASS and PlikTT[#]-Profile/CLASS.

As in the previous section, we have checked that the impact of the neutrino settings is almost negligible, as well as the impact of supernovae data. In addition, the choice of the DR12 BAO data instead of DR11 has no effect.

4.2. TE+lowTEB+BAO results

Given the *Planck* noise level, the TE likelihoods lead to similar results to those obtained with TT on Λ CDM. In addition they are less sensitive to the foreground modellings ([Galli et al. 2014](#); [Couchot et al. 2017a](#)). In this section we use the TE likelihood in place of the TT one and compare the results obtained on N_{eff} when combined with lowTEB and BAO in Table 6.

The remaining ΔN_{eff} is of the order of 0.07, which is small with respect to the total error with TE only. It may still contain some residual systematic uncertainty from temperature to polarisation leakage, the study of which is beyond the scope of this paper.

5. Conclusions

We have studied in detail the estimation of the effective number of relativistic species from CMB *Planck* data. We have tested different ingredients of the analysis to further quantify their impact on the results: mainly the Boltzmann codes, the high- ℓ likelihoods (Plik, HiLLiPOPps and CamSpec), and the statistical analysis.

Table 6. Results on N_{eff} obtained when combining BAO with PlikTE, and h1pTE.

<i>Planck</i> \mathcal{L}	Config	lowTEB
PlikTE	MCMC/CAMB	2.94 ± 0.37
h1pTE	Profile/CLASS	$3.01^{+0.32}_{-0.30}$

Notes. Errors are given at 68% CL. lowTEB has been used at low- ℓ .

- The estimated variation of N_{eff} when switching from CAMB to CLASS is negligible: of the order of $\Delta N_{\text{eff}} = 0.01$.
- If we can safely neglect the impact of the covariance matrix estimation, as suggested by the obtained results, the variation linked to the assumptions on foreground residuals modelling derived from the comparison of the high- ℓ likelihoods has been estimated to be of the order of $\Delta N_{\text{eff}} = 0.17$, of which a small part (up to 0.03) may be attributed to a statistical effect. We have also shown that, at least for HiLLiPOP, N_{eff} was mainly correlated with nuisance parameters linked to foregrounds playing a role at small scales (i.e. point sources and SZ).
- We have found slight differences between the Bayesian and the frequentist inferred mean values, linked to particular likelihood volume effects. A shift between both methods has been estimated to be $\Delta N_{\text{eff}} \leq 0.05$.

As an overall conclusion, we have shown that the variation of the mean N_{eff} values is non-negligible. This foreground related systematic uncertainty is of the same order of magnitude as the error derived for each individual likelihood. In addition the results obtained with HiLLiPOP and CamSpec lead systematically to lower values than the ones derived from the public *Planck* likelihood.

We have cross-checked the consistency of the results when considering TT and TE separately. When considering TE only (together with BAO and lowTEB), which is less sensitive to foreground residuals, this observed variation drops down to $\Delta N_{\text{eff}} = 0.05$ for the likelihoods we have been able to compare.

We have shown that likelihood modelling is an important challenge for the current *Planck* measurements for the N_{eff} interpretation, even for temperature data. The shift discussed in this paper is very large compared to the $\sigma(N_{\text{eff}}) = 0.027$ statistical-only expectations for CMB-S4. However, we expect data from the next generation of CMB experiments to be more robust to such systematic error. The increase in constraining power from the TE power spectrum with respect to the TT one, as well as the better determination of the temperature power spectrum on small scales, will reduce the impact of foreground mismodelling.

References

- Aad, G., Abbott, B., Abdallah, J., et al. 2014, *Phys. Rev. D*, **90**, 052004
- Abazajian, K. N., Arnold, K., Austermann, J., et al. 2015, *Astropart. Phys.*, **63**, 66
- Abazajian, K. N., Adshead, P., Ahmed, Z., et al. 2016, *CMB-S4 Science Book, First Edition*
- Alam, S., Ata, M., Bailey, S., et al. 2017, *MNRAS*, **470**, 2617
- Beringer, J., Arguin, J.-F., Barnett, R. M., et al. 2012, *Phys. Rev. D*, **86**, 010001
- Beutler, F., Saito, S., Brownstein, J. R., et al. 2014, *MNRAS*, **444**, 3501
- Binetruy, P., Deffayet, C., Ellwanger, U., & Langlois, D. 2000, *Phys. Lett. B*, **477**, 285
- Bird, S., Viel, M., & Haehnelt, M. G. 2012, *MNRAS*, **420**, 2551
- Blas, D., Lesgourgues, J., & Tram, T. 2011, *JCAP*, **7**, 034
- Blennow, M., Fernandez-Martinez, E., Mena, O., Redondo, J., & Serra, P. 2012, *JCAP*, **1207**, 022
- Calabrese, E., Slosar, A., Melchiorri, A., Smoot, G. F., & Zahn, O. 2008, *Phys. Rev. D*, **77**, 123531
- Calabrese, E., Huterer, D., Linder, E. V., Melchiorri, A., & Pagano, L. 2011, *Phys. Rev. D*, **83**, 123504
- Caramete, A., & Popa, L. 2014, *JCAP*, **1402**, 012
- Consiglio, R., de Salas, P. F., Mangano, G., et al. 2018, *Comput. Phys. Commun.*, **233**, 237
- Couchot, F., Henrot-Versillé, S., Perdereau, O., et al. 2017a, *A&A*, **602**, A41
- Couchot, F., Henrot-Versillé, S., Perdereau, O., et al. 2017b, *A&A*, **597**, A126
- Couchot, F., Henrot-Versillé, S., Perdereau, O., et al. 2017c, *A&A*, **606**, A104
- de Salas, P. F., & Pastor, S. 2016, *JCAP*, **7**, 051
- Fischler, W., & Meyers, J. 2011, *Phys. Rev. D*, **83**, 063520
- Flambaum, V., & Shuryak, E. 2006, *Europhys. Lett.*, **74**, 813
- Galli, S., Benabed, K., Bouchet, F., et al. 2014, *Phys. Rev. D*, **90**, 063504
- Haario, H., Saksman, E., & Tamminen, J. 2001, *Bernoulli*, **7**, 223
- Hamann, J. 2012, *JCAP*, **3**, 021
- Hamann, J., Hannestad, S., Raffelt, G. G., Tamborra, I., & Wong, Y. Y. 2010, *Phys. Rev. Lett.*, **105**, 181301
- Hannestad, S., Mirizzi, A., Raffelt, G. G., & Wong, Y. Y. 2010, *JCAP*, **1008**, 001
- Henrot-Versillé, S., Perdereau, O., Plaszczynski, S., et al. 2015, *Class. Quant. Grav.*, **32**, 045003
- Henrot-Versillé, S., Perdereau, O., Plaszczynski, S., et al. 2016, ArXiv e-prints [arXiv:1607.02964]
- Lesgourgues, J. 2011, ArXiv e-prints [arXiv:1104.2934]
- Lewis, A., Challinor, A., & Lasenby, A. 2000, *ApJ*, **538**, 473
- Mangilli, A., Plaszczynski, S., & Tristram, M. 2015, *MNRAS*, **453**, 3174
- Melchiorri, A., Mena, O., & Slosar, A. 2007, *Phys. Rev. D*, **76**, 041303
- Planck Collaboration XV. 2014, *A&A*, **571**, A15
- Planck Collaboration XVI. 2014, *A&A*, **571**, A16
- Planck Collaboration XI. 2016, *A&A*, **594**, A11
- Planck Collaboration XIII. 2016, *A&A*, **594**, A13
- Planck Collaboration Int. XXII. 2015, *A&A*, **576**, A107
- Planck Collaboration Int. XXX. 2016, *A&A*, **586**, A133
- Planck Collaboration Int. XLVII. 2016, *A&A*, **596**, A108
- Shiromizu, T., Maeda, K.-I., & Sasaki, M. 2000, *Phys. Rev. D*, **62**, 024012
- Smith, T. L., Pierpaoli, E., & Kamionkowski, M. 2006, *Phys. Rev. Lett.*, **97**, 021301
- Takahashi, R., Sato, M., Nishimichi, T., Taruya, A., & Oguri, M. 2012, *ApJ*, **761**, 152
- Tanabashi, M., Hagiwara, K., Hikasa, K., et al. 2018, *Phys. Rev. D*, **98**, 030001
- Tristram, M., Macías-Pérez, J. F., Renault, C., & Santos, D. 2005, *MNRAS*, **358**, 833

Appendix A: Appendix on nuisance parameters

This appendix presents the nuisance parameters of the HiLLiPOPps likelihood in Table A.1.

Table A.1. Nuisance parameters for the HiLLiPOPps likelihood.

Name	Definition
<i>Instrumental calibrations</i>	
$C_{100\text{hm}1}^{\text{Planck}}$	Map calibration (100-hm1)
$C_{100\text{hm}2}^{\text{Planck}}$	Map calibration (100-hm2)
$C_{143\text{hm}1}^{\text{Planck}}$	Map calibration (143-hm1)
$C_{143\text{hm}2}^{\text{Planck}}$	Map calibration (143-hm2)
$C_{217\text{hm}1}^{\text{Planck}}$	Map calibration (217-hm1)
$C_{217\text{hm}2}^{\text{Planck}}$	Map calibration (217-hm2)
A_{Planck}	Absolute calibration
<i>Foreground modellings</i>	
$A_{\text{PS}}^{\text{Planck}}(100 \times 100)$	PS amplitude in TT (100 × 100 GHz)
$A_{\text{PS}}^{\text{Planck}}(100 \times 143)$	PS amplitude in TT (100 × 143 GHz)
$A_{\text{PS}}^{\text{Planck}}(100 \times 217)$	PS amplitude in TT (100 × 217 GHz)
$A_{\text{PS}}^{\text{Planck}}(143 \times 143)$	PS amplitude in TT (143 × 143 GHz)
$A_{\text{PS}}^{\text{Planck}}(143 \times 217)$	PS amplitude in TT (143 × 217 GHz)
$A_{\text{PS}}^{\text{Planck}}(217 \times 217)$	PS amplitude in TT (217 × 217 GHz)
A_{radio}	Scaling for radio sources (TT)
A_{dusty}	Scaling for infrared sources (TT)
A_{SZ}	Scaling for the tSZ template (TT)
A_{CIB}	Scaling for the CIB template (TT)
A_{kSZ}	Scaling for the kSZ template (TT)
$A_{\text{SZ} \times \text{CIB}}$	Scaling for kSZ x CIB cross correlation
$A_{\text{dust}}^{\text{TT}}$	Scaling for the dust in TT
$A_{\text{dust}}^{\text{EE}}$	Scaling for the dust in EE
$A_{\text{dust}}^{\text{TE}}$	Scaling for the dust in TE